Stern-Gerlach Effect of Weak-Light Ultraslow Vector Solitons

Chao Hang and Guoxiang Huang

State Key Laboratory of Precision Spectroscopy and Department of Physics,
East China Normal University, Shanghai 200062, China
(Dated: September 4, 2012)

We propose a scheme to exhibit Stern-Gerlach (SG) deflection of high-dimensional vector optical soliton (VOS) at weak-light level in a cold atomic gas via electromagnetically induced transparency. We show that the propagating velocity and generation power of such VOS can be reduced to $10^{-6}\,c$ (c is light speed in vacuum) and lowered to magnitude of nanowatt, respectively. The stabilization of the VOS may be realized by using an optical lattice formed by a far-detuned laser field, and its trajectory can be deflected significantly by using a SG magnetic field. Deflection angle of the VOS can be of magnitude of 10^{-3} rad when propagating several millimeters. Different from atomic SG deflection, deflection angle of the VOS can be distinct for different polarization components and can be manipulated in a controllable way. The results obtained can be described in terms of a SG effect for the VOS with quasispin and effective magnetic moment.

Stern-Gerlach (SG) effect, i.e., a particle with nonzero magnetic moment deflects when passing through an inhomogeneous magnetic field, was firstly discovered in early time of quantum mechanics. This effect illustrates the necessity for a radical departure from classical mechanics, and characterizes quantum nature of atomic motion in a simple and fundamental way [1]. Recently, similar effect was also predicted in many other systems, e.g., spinor Fermi and Bose gases [2] and chiral molecules [3].

All massive elementary particles, such as electrons, have non-zero magnetic moments. Contrarily, photons have no magnetic moment in vacuum, thus experience no force when passing through inhomogeneous magnetic field. Recently, in a very remarkable experiment [4], Karpa and Weitz showed that photons may acquire effective magnetic moments when propagating in a resonant atomic gas, and hence can deflect by a gradient magnetic field. In their experiment, a technique of electromagnetically induced transparency (EIT) [5] is exploited, by which a small absorption and slow propagating velocity of photons can be realized.

However, the EIT-enhanced deflection of light in Ref. [4] cannot be explained as a standard SG effect because only one component of "spin" is involved. In this Letter, we propose a double EIT scheme to demonstrate a SG effect of high-dimensional vector optical soliton (VOS), which not only has two polarization components (i.e. a quasispin) but also allows a distortionless propagation. Propagating velocity and generation power of the VOS can be reduced to very low level. Stabilization of the VOS can be realized using an optical lattice formed by a far-detuned laser field. The VOS can acquire very large effective magnetic moments, and the deflection of its trajectory is much more significant when passing though a SG gradient magnetic field.

Before proceeding, we note that besides Ref. [4], optical beam deflection in external fields has been the subject of many previous works [6–10]. The present work is re-

lated to Refs. [4, 9, 10] and to recent studies of slow-light solitons [11–13]. Essence of Refs. [4, 9, 10] is a SG effect of linear polaritons. However, such linear polaritons spread and attenuate during propagation because of the existence of diffraction and other detrimental effects. In Refs. [11–13], slow-light solitons via EIT are suggested, but no SG effect is considered.

In contrast, the scheme presented here exploits optical lattice and EIT-enhanced Kerr effect, which allow the formation and stable propagation of high-dimensional VOS, or called *nonlinear polariton*, with effective magnetic moment (SG deflection) being four (two) orders of magnitude larger than that of the linear polariton of Ref. [4]. Thus, comparing with that obtained in a linear scheme [4, 9, 10], the SG effect proposed here is more efficient and robust for observation and practical applications.

To be specific, we consider a medium consisting of five-level atoms with M-configuration. A linearly polarized, pulsed probe field (with pulse duration τ_0) $\mathbf{E}_p = \mathbf{E}_{p1} + \mathbf{E}_{p2} = (\hat{\epsilon}_-\mathcal{E}_{p1} + \hat{\epsilon}_+\mathcal{E}_{p2})\exp[i(k_p z - \omega_p t)] + \text{c.c.}$ drives the transitions $|3\rangle \leftrightarrow |2\rangle$ and $|3\rangle \leftrightarrow |4\rangle$ by its left-circular (i.e. σ^-) polarization component $\mathbf{E}_{p1}$ and right-circular (i.e. σ^+) polarization component $\mathbf{E}_{p2}$, respectively. Here $\mathcal{E}_{p1,p2}$ are envelopes and $\hat{\epsilon}_\pm \equiv (\hat{\mathbf{x}}\pm i\hat{\mathbf{y}})/\sqrt{2}$. A π-polarized, strong continuous-wave control field $\mathbf{E}_{c1} = \hat{\mathbf{z}}\mathcal{E}_{c1}\exp[i(k_{c1}x - \omega_{c1}t)] + \text{c.c.}$ ($\mathbf{E}_{c2} = \hat{\mathbf{z}}\mathcal{E}_{c2}\exp[i(k_{c2}x - \omega_{c2}t)] + \text{c.c.}$) drives the transition $|1\rangle \leftrightarrow |2\rangle$ ($|5\rangle \leftrightarrow |4\rangle$) (Fig. 1(a)). $\hat{\mathbf{x}}$, $\hat{\mathbf{y}}$, and $\hat{\mathbf{z}}$ are unit vectors along coordinate axes x, y and z, respectively (Fig. 1(b)).

We assume an inhomogeneous magnetic field $\mathbf{B}(y) = \hat{\mathbf{z}}B(y) = \hat{\mathbf{z}}(B_0 + B_1 y)$ ($B_1 \ll B_0$) is applied to the system. Here B_0 contributes to a Zeeman level shift $\Delta E_Z = \mu_B g_F^j m_F^j B_0$, and hence removes the degeneracy of ground-state sublevels $|j\rangle$ ($j = 1, 3, 5$) and the excited-state sublevels $|l\rangle$ ($l = 2, 4$). μ_B, g_F^j, and m_F^j are Bohr magneton, gyromagnetic factor, and magnetic quantum number of the level $|j\rangle$, respectively. B_1 contributes a transverse gradient of the magnetic field, resulting in a
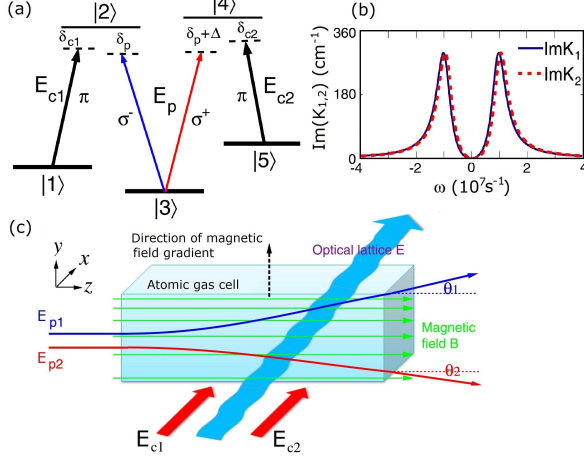
FIG. 1: (color online) (a): Double EIT scheme. $\mathbf{E}_p$ and $\mathbf{E}_{cj}$ ($j = 1, 2$) are probe and control fields, respectively; δ_p, $\delta_p + \Delta$, and δ_{cj} are detunings. (b): Absorption spectrum $\mathrm{Im}K_j(\omega)$ as functions of ω. Solid and dotted lines correspond to the σ^- and σ^+ polarization components, respectively. (c): A possible experimental arrangement, where an inhomogeneous magnetic field $\mathbf{B}$ removes the degeneracy of ground states $|j\rangle$ ($j = 1, 3, 5$) and excited states $|l\rangle$ ($l = 2, 4$), and causes Stern-Gerlach deflection of probe-field components. θ_1 and θ_2 are deflection angles of σ^- polarization component (i.e. $\mathbf{E}_{p1}$) and σ^+ polarization component (i.e. $\mathbf{E}_{p2}$) of high-dimensional VOS, which has a quasispin and an effective magnetic moment. The curved thick arrow represents the far-detuned optical lattice field $\mathbf{E}$ used to stabilize the VOS.

SG deflection of the probe field.

We assume further a small, far-detuned laser field $\mathbf{E}(x, t) = \hat{\mathbf{x}}E_0 \cos(x/R_\perp) \cos(\omega_L t)$ is also applied into the medium, where E_0, $R_\perp$, and ω_L are field amplitude, beam radius, and angular frequency, respectively. Due to $\mathbf{E}(x, t)$, Stark level shift $\Delta E_{j,\mathrm{S}} = -\frac{1}{2}\alpha_j \langle E^2 \rangle_t = -\frac{1}{2}\alpha_j E^2(x)$ occurs, here α_j is the scalar polarizability of the level $|j\rangle$, $\langle \cdots \rangle_t$ denotes the time average in an oscillation cycle, and hence $E(x) = (E_0/\sqrt{2}) \cos(x/R_\perp)$. The aim of introducing the far-detuned laser field is to form an optical lattice potential to stabilize the high-dimensional VOS [14], as shown below.

Besides, atoms are assumed prepared initially in the ground-state level $|3\rangle$ and trapped in a gas cell with ultracold temperature to cancel Doppler broadening and collisions. Thus, the system is composed of two Λ-type EIT configurations (i.e. double EIT). A possible arrangement of experimental apparatus is suggested in Fig. 1(c).

Under electric-dipole and rotating-wave approximations, the Hamiltonian of the system in interaction picture is $H_{\mathrm{int}}/\hbar = (\delta_p - \delta_{c1})|1\rangle\langle 1| + \delta_p|2\rangle\langle 2| + (\delta_p + \Delta)|4\rangle\langle 4| + (\delta_p + \Delta - \delta_{c2})|5\rangle\langle 5| + \Omega_{c1}|2\rangle\langle 1| + \Omega_{p1}|2\rangle\langle 3| + \Omega_{p2}|4\rangle\langle 3| + \Omega_{c2}|4\rangle\langle 5| + \mathrm{H.c.}$, where $\Omega_{p1} = -(\mathbf{p}_{23} \cdot \hat{\epsilon}_-)\mathcal{E}_{p1}/\hbar$ and $\Omega_{p2} = -(\mathbf{p}_{43} \cdot \hat{\epsilon}_+)\mathcal{E}_{p2}/\hbar$ ($\Omega_{c1} = -(\mathbf{p}_{21} \cdot \hat{\mathbf{z}})\mathcal{E}_{c1}/\hbar$ and $\Omega_{c2} = -(\mathbf{p}_{45} \cdot \hat{\mathbf{z}})\mathcal{E}_{c2}/\hbar$) are respectively Rabi frequencies of two circularly polarized components of the probe field (two π-polarized control fields), with $\mathbf{p}_{jl}$ being the electric dipole matrix element associated with the transi-

tion from $|j\rangle$ to $|l\rangle$. The detunings are defined as $\delta_p = \omega_{23} + \mu_{23}B(y) - \frac{1}{2}\alpha_{23}E(x)^2 - \omega_p$, $\delta_{c1} = \omega_{21} + \mu_{21}B(y) - \frac{1}{2}\alpha_{21}E(x)^2 - \omega_{c1}$, $\delta_{c2} = \omega_{45} + \mu_{45}B(y) - \frac{1}{2}\alpha_{45}E(x)^2 - \omega_{c2}$, and $\Delta = \mu_{42}B(y) - \frac{1}{2}\alpha_{42}E(x)^2$, where $\mu_{jl} = \mu_B(g_F^j m_F^j - g_F^l m_F^l)/\hbar$, $\alpha_{jl} = (\alpha_j - \alpha_l)/\hbar$, and $\omega_{jl} = (E_j - E_l)/\hbar$, with E_j being the eigenenergy of the state $|j\rangle$.

The motion of atoms is governed by the Bloch equation for density-matrix ρ,

$$\partial\rho/\partial t = -i[H_{\mathrm{int}}, \rho]/\hbar - \Gamma(\rho), \qquad (1)$$

where $\Gamma(\rho)$ is relaxation matrix representing spontaneous emission and dephasing (see Supplementary Material). Electric-field evolution is controlled by Maxwell equation

$$\nabla^2\mathbf{E} - (1/c^2)\partial^2\mathbf{E}/\partial t^2 = (1/\epsilon_0 c^2)\partial^2\mathbf{P}/\partial t^2, \qquad (2)$$

where $\mathbf{P} = \mathcal{N}\mathrm{Tr}(\mathbf{p}\rho)$ is electric polarization with $\mathcal{N}$ the atomic density. Under slowly varying envelope approximation, Eq. (2) reduces to $[i\partial_z + (i/c)\partial_t + c\nabla_\perp^2/(2\omega_p)]\Omega_{p1,p2} - \kappa_{32,34}\rho_{23,43} = 0$, where $\nabla_\perp^2 = \partial^2/\partial x^2 + \partial^2/\partial y^2$ and $\kappa_{32,34} = \mathcal{N}|\mathbf{p}_{32,34} \cdot \hat{\epsilon}_\mp|^2\omega_p/(2\hbar\epsilon_0 c)$ with ϵ_0 the vacuum dielectric constant.

Linear propagation of the probe field in the absence of diffraction can be obtained by taking $\Omega_{p1,p2}$ as small quantities and B_1, E_0 as zero. Then one has $\Omega_{pj} = F_j \exp\{i[K_j(\omega)z - \omega t]\}$ ($j = 1, 2$) with $K_{1,2}(\omega) = \omega/c + \kappa_{32,34}(\omega - d_{1,5})/D_{1,2}$ (linear dispersion relation). Here, F_j are constants, $D_{1,2} = |\Omega_{c1,c2}|^2 - (\omega - d_{1,5})(\omega - d_{2,4})$, $d_1 = (\delta_p - \delta_{c1}) - i\gamma_{13}/2$, $d_2 = \delta_p - i(\Gamma_2 + \gamma_{23})/2$, $d_4 = (\delta_p + \Delta) - i(\Gamma_4 + \gamma_{34})/2$, and $d_5 = (\delta_p + \Delta - \delta_{c2}) - i\gamma_{35}/2$ with $\delta_p = \omega_{23} + \mu_{23}B_0 - \omega_p$, $\Delta = \mu_{42}B_0$, $\delta_{c1} = \omega_{21} + \mu_{21}B_0 - \omega_{c1}$, and $\delta_{c2} = \omega_{45} + \mu_{45}B_0 - \omega_{c2}$. Γ_i and γ_{ij} denote the spontaneous emission and dephasing rates of relevant states, respectively.

The linear dispersion relation displays two branches. Fig. 1(b) shows the absorption spectrum of $\mathrm{Im}K_j(\omega)$ ($j = 1, 2$) as a function of frequency ω. Parameters are chosen for a laser-cooled $^{85}\mathrm{Rb}$ atomic gas with $|1\rangle = |5^2S_{1/2}, F = 2, m_F = -1\rangle$, $|2\rangle = |5^2P_{1/2}, F = 2, m_F = -1\rangle$, $|3\rangle = |5^2S_{1/2}, F = 1, m_F = 0\rangle$, $|4\rangle = |5^2P_{1/2}, F = 2, m_F = 1\rangle$, and $|5\rangle = |5^2S_{1/2}, F = 2, m_F = 1\rangle$. Decay rates are $\Gamma_2 \simeq \Gamma_4 \simeq 6$ MHz and $\gamma_{13} \simeq \gamma_{23} \simeq \gamma_{34} \simeq \gamma_{35} \simeq 50$ Hz. Other parameters are taken as $\kappa_{32} \simeq \kappa_{34} = 1.0 \times 10^9$ cm^{-1}s^{-1}, $\Omega_{c1} = \Omega_{c2} = 1.0 \times 10^7$ s^{-1}, $\delta_p = \delta_{c1} = \delta_{c2} = 0$, and $B_0 = 34.1$ mG. The solid (dotted) line in the figure is for σ^- (σ^+) polarization component. We see that large and deep transparency windows in the absorption spectra of both polarization components (double EIT) appear. Using above parameters, group velocities of the both components (defined by $V_{gj} = \mathrm{Re}(\partial K_j/\partial\omega)^{-1}$) are given as $3.3 \times 10^{-6}c$.

However, the linear solution is unstable due to the diffraction and other detrimental effects, which results in spreading and attenuation of the probe field during propagation, as demonstrated by Eq. (24) of Ref. [10].

To solve this problem we use nonlinear effect to suppress the spreading and attenuation. When including weak nonlinearity and diffraction, we obtain the following nonlinearly coupled, dimensionless equations, derived by using a standard method of multiple-scales (see the Supplementary Material):

$$\left[\frac{i}{v_{g1,g2}}\frac{\partial}{\partial \tau} + \frac{1}{2}\left(\frac{\partial^2}{\partial \xi^2} + \frac{\partial^2}{\partial \eta^2}\right)\right]u_{1,2} - \frac{1}{\sqrt{2\pi}\rho_0}(g_{11,22}|u_{1,2}|^2$$
$$+g_{12,21}|u_{2,1}|^2)u_{1,2} + V_{1,2}(\xi,\eta)u_{1,2} = -iA_{1,2}u_{1,2}. \quad (3)$$

where $\tau = t/\tau_0$, $(\xi,\eta) = (x,y)/R_\perp$, $v_{gj} = V_{gj}\tau_0/L_{\text{Diff}}$, and $u_j(\tau,\xi,\eta) = [\Omega_{pj}/F_j(\rho_j)]e^{-i\text{Re}[K_j|_{\omega=0}]z}/U_0$. Here, $L_{\text{Diff}} = \omega_p R_\perp^2/c$ and U_0 are respectively the typical diffraction length and Rabi frequency, $F_j(\rho_j)$ are normalized Gaussian functions (i.e. $F_j = [1/(\rho_0\sqrt{\pi})]^{1/2}\exp[-\rho_j^2/(2\rho_0^2)]$ with $\rho_j = (z - V_{gj}t)/L_{\text{Diff}}$ and ρ_0 a constant [10]), $g_{11,12,21,22} = W_{11,12,21,22}/|W_{22}|$ are nonlinearity coefficients with $W_{11,22} = -\kappa_{32,34}d_{1,5}(|d_{1,5}|^2 + |\Omega_{c1,c2}|^2)/(D_{1,2}|D_{1,2}|^2)$ and $W_{12,21} = -\kappa_{32,34}d_{1,5}(|d_{5,1}|^2 + |\Omega_{c2,c1}|^2)/(D_{1,2}|D_{2,1}|^2)$ characterizing respectively self-phase and cross-phase modulations, and $A_j = \text{Im}[K_j|_{\omega=0}]L_{\text{Diff}}$ are small absorption coefficients.

Combined potentials in Eq. (3) have the form

$$V_j(\xi,\eta) = \mathcal{M}_j\eta + \mathcal{N}_j\cos^2(\xi), \quad (4)$$

where $\mathcal{M}_{1,2} = M_{1,2}R_\perp B_1$ and $\mathcal{N}_{1,2} = N_{1,2}E_0^2$ are contributions from the SG gradient magnetic field (proportional to B_1) and the optical lattice field (proportional to E_0^2), respectively. M_j and N_j are defined as $M_{1,2} = -\kappa_{32,34}(d_{1,5}^2\mu_{23,43} + |\Omega_{c1,c2}|^2\mu_{13,53})L_{\text{Diff}}/D_{1,2}^2$ and $N_{1,2} = \frac{1}{4}\kappa_{32,34}(d_{1,5}^2\alpha_{23,43} + |\Omega_{c1,c2}|^2\alpha_{13,53})L_{\text{Diff}}/D_{1,2}^2$. When deriving Eq. (3), B_1 and E_0^2 are assumed as small quantities. Additionally, τ_0 is also assumed to be large (e.g. $\tau_0 = 2.1$ μs) so that the second-order dispersion (proportional to $\partial^2 u_j/\partial\tau^2$) is negligible.

Fig. 2 (a) and (b) show results of numerical simulation for $|u_1|^2$ respectively at $t = 0$ and $t = 3\tau_0$ for a deep optical lattice ($E_0 = 3.2\times 10^4$ V cm^{-1}). The soliton obtained displays a single-peaked structure. The result for $|u_2|^2$ is similar to $|u_1|^2$ due to symmetry and hence not shown. The case for a shallower optical lattice ($E_0 = 2.3\times 10^4$ V cm^{-1}) is also simulated, with the result plotted in panels (c) and (d) for $t = 0$ and $t = 3\tau_0$, respectively. We see that in this case a multiple-peaked soliton appears. In both simulations, $\delta_p = 1.0\times 10^6$ s^{-1}, $\delta_{c2} = 1.0\times 10^5$ s^{-1}, and $R_\perp = 16$ μm with other parameters the same with those in Fig. 1. In addition, $U_0 = 6.8\times 10^6$ s^{-1}, which allows enough nonlinearity to balance the diffraction. The typical diffraction length L_{Diff} and nonlinearity length L_{Nonl} ($\equiv 1/(U_0^2|W_{22}|)$) are $\simeq 0.2$ cm. Furthermore, B_1 is chosen as zero, i.e., the SG gradient magnetic field is absent, thus no SG deflection occurs.

The stability of the high-dimensional VOS is checked by adding a small random perturbation to the stationary
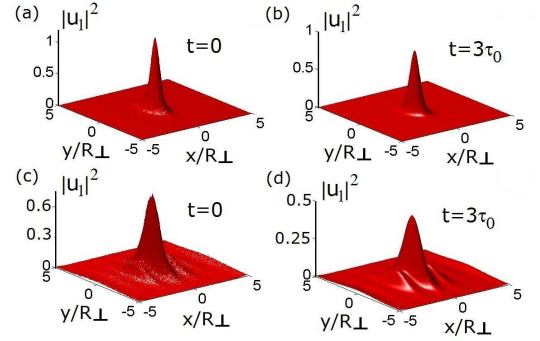

FIG. 2: (color online) (a) and (b): Evolutions of $|u_1|^2$ respectively at $t = 0$ and $t = 3\tau_0$ for single-peaked VOS. (c) and (d): Evolutions of $|u_1|^2$ respectively at $t = 0$ and $t = 3\tau_0$ for multiple-peaked VOS. SG gradient magnetic field is absent (i.e. $B_1 = 0$). The stability of the VOS is achieved by the far-detuned optical lattice. Result for $|u_2|^2$ is similar to $|u_1|^2$ thus not shown.
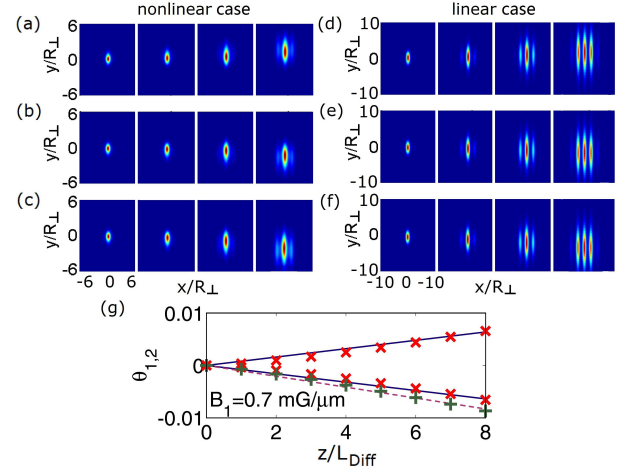

FIG. 3: (color online) SG effect of ultraslow VOS. (a) and (b): Symmetric deflection (on y-axis) of $|u_1|^2$ and $|u_2|^2$ when propagating from $z = 2L_{\text{Diff}}$ to $z = 8L_{\text{Diff}}$ (corresponding respectively to the subfigure from left to right), respectively. (c): Asymmetric deflection of $|u_2|^2$ ($|u_1|^2$ is the same as (a) thus not shown). (d), (e), (f): Corresponding evolution of linear polariton. (g): Deflection angles of the VOS as functions of z/L_{Diff} for $B_1 = 0.7$ mG/μm. The solid line with positive (negative) slope is the analytical result of θ_1 (θ_2) for the symmetric case. Dashed line is the analytical result of θ_2 for the asymmetric case (θ_1 is the same as the symmetric case thus not shown). Points labeled by "x" and "+" are center positions of the VOS polarization components obtained numerically.

solution obtained in imaginary time (Fig. 2 (a), (c)) and evolving the solution according to Eq. (3) in real time. We find that the soliton can indeed propagate stably for a long time (Fig. 2 (b), (d)). We have also used a standard linear stability analysis (see the Supplementary Material) to confirm the stability of the high-dimensional VOS.

Next we study VOS deflection by numerically simulating Eq. (3) with $B_1 \neq 0$. Shown in Fig. 3 (a) and (b) are spatial distributions of $|u_1|^2$ (panel (a)) and $|u_2|^2$ (panel (b)) in (x,y)-plane when the VOS propa-

gates from $z = 2L_{\text{Diff}}$ to $z = 8L_{\text{Diff}}$ with group velocity $V_{g1} \simeq V_{g2} = 3.2 \times 10^{-6}c$. In the simulation, $B_1 = 0.7$ mG μm^{-1} is chosen. We see that an obvious deflection of VOS trajectories occurs due to the existence of the SG gradient magnetic field. Additionally, two different polarization components deflect symmetrically in $+y$ and $-y$ directions, similar to the SG deflection for atoms.

The SG deflection of VOS components can be made asymmetric. To show this, we take $\Omega_{c2} = 0.9 \times 10^7$ s^{-1} without changing other parameters, then $(V_{g1}, V_{g2}) = (3.2, 2.6) \times 10^{-6}c$. As a result, the trajectory of σ^- component keeps unchanged, whereas the trajectory of σ^+ component changes as shown in Fig. 3(c). This is different from atomic SG deflection, where trajectories are always symmetric for two different spin components.

For comparison, in Fig. 3(d), (e), and (f) we present results of corresponding evolution for a linear polariton. One sees that the probe pulse spread rapidly. Thus the nonlinear effect is necessary for obtaining stable VOS and its robust SG deflection.

Analytical VOS solutions of Eq. (3) can be gained under some approximations: (i)The small absorption term $-iA_j u_j$ is disregarded. (ii)Since in the presence of the SG gradient magnetic field the two polarization components of VOS separate each other after propagating some distance, the cross-phase-modulation terms can be neglected. (iii)The optical lattice is deep enough so that V_j can be approximated as $\mathcal{M}_j\eta + \mathcal{N}_j(1 - \xi^2)$. Taking $u_j(\tau,\xi,\eta) = w_j(\tau,\eta)\phi_j(\xi)\exp[i\mathcal{N}_j v_{gj}\tau]$, where $\phi_j(\xi)$ is the normalized ground state of the eigenvalue problem $(\partial^2/\partial\xi^2 - 2\mathcal{N}_j\xi^2)\phi_j = 2E_\xi\phi_j$ with $E_\xi = -\sqrt{\mathcal{N}_j/2}$, and integrating out the variable ξ, Eq. (3) reduces to $[(i/v_{gj})\partial_\tau + (1/2)\partial_\eta^2]w_j - \mathcal{N}_j^{1/4}/(2^{3/4}\pi\rho_0)g_{jj}|w_j|^2 w_j + (\mathcal{M}_j\eta - \sqrt{\mathcal{N}_j/2})w_j = 0$, which admits exact soliton solutions [15]. A single-soliton solution (see the Supplementary Material) gives

$$\Omega_{pj} = U_0 A_j [1/(\rho_0\sqrt{\pi})]^{1/2} (\sqrt{2\mathcal{N}_j}/\pi)^{1/4} e^{i\varphi_j}$$
$$\times e^{-(s-v_{gj}\tau)^2/(2\rho_0^2)} e^{-\sqrt{\mathcal{N}_j}\xi^2/\sqrt{2}}\text{sech}\Theta_j, \quad (5)$$

where $A_j = (2^{5/4}\mathcal{N}_j^{1/4}\pi\rho_0/|g_{jj}|)^{1/2}$, $\varphi_j = \mathcal{M}_j v_{gj}\tau(\eta - \mathcal{M}_j v_{gj}^2\tau^2/6)$, and $\Theta_j = (2\mathcal{N}_j)^{1/4}(\eta - \mathcal{M}_j v_{gj}^2\tau^2/2)$ ($j = 1,2$). We see that both VOS components are localized in three spatial and one temporal dimensions. Thus, (u_1, u_2) can be considered as a *vector light bullet*.

After passing the medium with length L, the center position of the jth polarization component of the VOS is at $(x, y_j, z) = (0, \mathcal{M}_j L^2 R_\perp/(2L_{\text{diff}}^2), L)$, with the propagating velocity along the z- (y-) direction given by V_{gj} ($V_j \equiv \mathcal{M}_j v_{gj}^2 R_\perp t/\tau_0^2$). As a result, the expected deflection angle of the jth VOS component is

$$\theta_j = V_j/V_{gj} = (L/V_{gj})(\mu_{\text{sol}\,j}/p)r^2 B_1, \quad (6)$$

where $r = R_\perp/L_{\text{Diff}}$, $p = \hbar k_p$ is photon momentum, $\mu_{\text{sol}\,j} = M_j V_{gj}\hbar k_p$ is effective magnetic moment. With

the data in Fig. 3, we obtain $\mu_{\text{sol}\,1,2} = \pm 7.6 \times 10^{-20}$ J/T, which is four orders of magnitude larger than the effective magnetic moment for linear polariton of Ref. [4]. From Eq. (6) we see the deflection angle of the jth polarization component of the VOS is proportional to the medium length L, the SG gradient magnetic field B_1, and inversely proportional to the group velocity V_{gj}. In a mechanical viewpoint, the deflection of the jth component of the VOS is caused by the transverse magnetic force $F_j = \mu_{\text{sol}\,j}B_1$ and deflection angles can be expressed as $\theta_j = F_j t_{\text{int}\,j}r^2/p_j$ with $t_{\text{int}\,j} = L/V_{gj}$ being the interaction time. Due to untraslow propagating velocity, large deflection angles may be observed even for small L.

Fig. 3(g) shows deflection angles of the VOS as functions of z/L_{Diff} for $B_1 = 0.7$ mG/μm. The solid line of positive (negative) slope is the analytical result of θ_1 (θ_2) by Eq. (6) for the σ^- (σ^+) component with $V_{g1} \simeq V_{g2} = 3.3 \times 10^{-6}c$ (i.e. the symmetric case). Points labeled by "x" are center positions of the VOS components obtained numerically. We thus have $(\theta_1, \theta_2) \simeq (1.6, -1.6) \times 10^{-3}$ rad for $z = 0.4$ cm, which is two orders of magnitude larger than that for linear polariton obtained in Ref. [4]. The dashed line is the analytical result of θ_2 with $(V_{g1}, V_{g2}) = (3.2, 2.6) \times 10^{-6}c$ (i.e. the asymmetric case) and points labeled by "+" are numerical results (θ_1 is the same as the symmetric case). In both cases analytical results agree well with numerical ones.

The generation power of the high-dimensional VOS predicted above can be estimated by using Poynting's vector [12], which is 3.5 nW calculated using the above parameters. Thus, very low input power is needed for generating the VOS in the present double EIT system.

In conclusion, a scheme is proposed to exhibit SG deflection of high-dimensional VOS via a double EIT. The VOS has ultraslow propagating velocity and extremely low generation power. The stabilization of the VOS can be realized by using an optical lattice, and its trajectory can be significantly deflected by a SG gradient magnetic field. The results obtained can be described in terms of a SG effect of the VOS with quasispin and effective magnetic moments. We expect that such large and robust SG effect may have potential applications in magnetometry and quantum information processing.

[1] J. J. Sakurai, *Modern Quantum Mechanics* (Revised Edition) (Addison-Wesley, 1994).
[2] M. D. Girardeau and M. Olshanii, Phys. Rev. A **70**, 023608 (2004).
[3] Y. Li *et al.*, Phys. Rev. Lett. **99**, 130403 (2007).
[4] L. Karpa and M. Weitz, Nat. Phys. **2**, 332 (2006).
[5] M. Fleischhauer *et al.*, Rev. Mod. Phys. **77**, 633 (2005).
[6] R. Schlesser and A. Weis, Opt. Lett. **17**, 1015 (1992).

[7] R. Holzner *et al.*, Phys. Rev. Lett. **78**, 3451 (1997).

[8] G. T. Purves *et al.*, Eur. Phys. J. D **29**, 433 (2004).

[9] D. L. Zhou *et al.*, Phys. Rev. A **76**, 055801 (2007).

[10] Y. Guo *et al.*, Phys. Rev. A **78**, 013833 (2008).

[11] Y. Wu and L. Deng, Phys. Rev. Lett. **93**, 143904 (2004).

[12] G. Huang *et al.*, Phys. Rev. E **72**, 016617 (2005).

[13] H. Michinel *et al.*, Phys. Rev. Lett. **96**, 023903 (2006).

[14] B. B. Baizakov *et al.*, Phys. Rev. A **70**, 053613 (2004).

[15] J. Yan *et al.*, Phys. Fluids A **4**, 690 (1992).